Fine-structure branching in the near-threshold photodissociation of NaK($X\ ^1\Sigma^+ - B\ ^1\Pi$)

J. X. Wang and P. D. Kleiber
Department of Physics and Astronomy, The University of Iowa, Iowa City, Iowa 52242-1479

K. M. Sando and W. C. Stwalley*
Department of Chemistry, The University of Iowa, Iowa City, Iowa 52242-1479
(Received 9 July 1990)

We have measured the $X\ ^1\Sigma^+ - B\ ^1\Pi$ bound-free molecular photodissociation profile of NaK under molecular-beam conditions. The dissociation results in excited $K^*(4\ ^2P)$. We have measured the D_1/D_2 fine-structure branching ratio; this ratio is a strong function of wavelength ranging from near zero to $D_1/D_2 \simeq 25\%$ as the laser is tuned through the bound-free absorption profile.

I. INTRODUCTION

Molecular photodissociation leading to excited photofragments has been a subject of interest in recent years, in part because of the insight it allows into excited-state collision dynamics.[1-4] Photodissociation processes can be described as a "half-collision" analog of full state-to-state collision experiments. Photodissociation studies, however, can have distinct advantages over gas-cell or crossed-beam experiments in some cases. The half-collision starts with a relatively narrow range of angular momenta (impact parameters). In many instances the system can be prepared in a well-defined electronic state. In direct photodissociation processes the collision energy can be "tuned" by tuning the dissociation laser frequency near threshold, and in the absence of barriers, this collision energy can be tuned aribitrarily close to threshold.

The final asymptotic distribution of fragment states resulting from the initially prepared molecular state will be determined by the adiabatic correlation and nonadiabatic mixing during the dissociation. This mixing results from effects such as spin-orbit interactions, rotational coupling, etc. The collision energy can be varied over a wide range in comparison to the strengths of these various molecular interactions. These experiments can give detailed insight into the importance of such couplings on the dissociation as a function of energy. Thus, measurements of the detailed fragment state distribution allow a sensitive probe of the excited-state half-collision dynamics.

There has been significant effort expended in measurements of the final distribution of electronic levels and fine-structure states following photodissociation of the homonuclear alkali-metal diatomics.[5-19] One advantage of these systems is the availability of reliable potential-energy curves.[20-23] Photodissociation of K_2 via the $B\ ^1\Pi_u$ state, for example, is adiabatic leading exclusively to the $K^*(4\ ^2P_{3/2}(D_2))$ level.[15] For Na_2, however, this process leads to a significant branching into the $Na^*(3\ ^2P_{1/2}(D_1))$ level.[7,10,15] This degree of mixing is higher than should be expected on the basis of nonadiabatic spin-orbit coupling alone.[18] The usual explanation for this result assumes some direct photodissociation via the $A\ ^1\Sigma_u^+$ state which adiabatically correlates with the $Na^*(3\ ^2P_{1/2}(D_1))$ level. The Franck-Condon factors for this process are quite unfavorable.

Studies of the photodissociation of the heteronuclear alkali-metal diatomics allows an important comparison with the homonuclear case. Here we report on measurements of the direct photodissociation of NaK. The process may be described

$$\mathrm{NaK}(X\ ^1\Sigma^+) + h\nu_L\ (\approx 560\ \mathrm{nm}) \rightarrow \mathrm{NaK}^*(B\ ^1\Pi) \rightarrow \mathrm{Na}(3\ ^2S) + K^*(4\ ^2P_J)\ .$$

The molecular-state symmetries and the atomic product state are identical to the homonuclear K_2 case [with the possibly important exception of the nuclear exchange $(g-u)$ symmetry]. However, there are significant differences in the long-range form of the interaction. The $K_2^*(B\ ^1\Pi_u)$ state is predominantly a repulsive R^{-3} form at long range while the $NaK^*(B\ ^1\Pi)$ state is predominantly an attractive R^{-6} form at long range. This major difference has two important consequences: (1) the region of nonadiabatic mixing will be at much smaller internuclear separation in the heteronuclear case; and (2) there is no natural barrier limiting the approach to threshold.

In the discussion of K_2 the spin-orbit mixing is strongest in the region near $R \approx 45a_0[\approx (C_3/E_{\mathrm{s.o.}})^{1/3}]$ while for NaK the spin-orbit coupling should become significant in the range $R \approx 17a_0[\approx (C_6/E_{\mathrm{s.o.}})^{1/6}]$. Similarly, the rotational coupling will become significant at much smaller internuclear separations. These differences may have a large influence on the degree of mixing, and, therefore, on the final-state distribution. Furthermore, in the photodissociation of K_2, the natural $B\ ^1\Pi_u$ state barrier limits the final-state kinetic energy to $\gtrsim 300\ \mathrm{cm}^{-1}$. In the heteronuclear NaK case there is no such natural barrier and we are able to tune arbitrarily close to threshold.

We have measured the $X\ ^1\Sigma^+ - B\ ^1\Pi$ bound-free molecular photodissociation profile of NaK under molecular-beam conditions. The profile extends over a range from 550–580 nm, peaking near 560 nm. We have also measured the nascent D_1/D_2 fine-structure branching ratio.

This process is the half-collision analog of Na+K* fine-structure changing collisions.[24] In contrast to the K_2 case where no D_1 emission was observed,[15,19] photodissociation of NaK leads to a significant D_1/D_2 branching which is a strong function of wavelength. The result ranges from nearly adiabatic ($D_1/D_2 \simeq 0$) to $D_1/D_2 \simeq 25\%$ as the laser is tuned through the bound-free profile. This branching ratio is unexpectedly large in comparison with semiclassical model predictions including both spin-orbit and rotational coupling.

II. EXPERIMENT

The NaK effusive molecular beam was produced by resistively heating a mixture of Na and K ($\sim$1:4) in a stainless-steel oven ($T_0 \sim 720$ K). The vapor expanded through a superheated 0.5-mm nozzle into a stainless-steel vacuum chamber with a background pressure under operating conditions of $\sim 1\times10^{-4}$ Torr. A 4-W Ar^+ laser (Innova 70-4) pumped a tunable broadband cw dye laser (CR-599) operated with Rhodamine 560 laser dye. The unfocused laser beam (power $\sim$100 mW) was chopped at $\sim$1 kHz and directed into the vacuum system to cross the NaK molecular beam at right angles $\sim$8 mm downstream from the nozzle. Excitation from the ground $X\,^1\Sigma^+$ state into the continuum of the $B\,^1\Pi$ state produces excited atomic $K^*(4\,^2P_J)$. Emission from the fine-structure states was detected with a filtered photomultiplier tube (EMI 9658). Narrow bandpass filters [1 nm full width at half maximum (FWHM)] were used to resolve the D_1 and D_2 resonance line emissions at 770 and 766 nm, respectively. The phototube output was detected with a lockin amplifier (SRS 570).

The bound-free excitation profiles leading to D_2 and D_1 emission are shown in Fig. 1. There is slight evidence for structure in the D_2 profile between 565 and 570 nm which might be associated with excitation to bound or quasibound states.[13] Heavy thermal averaging and poor spectral resolution make detailed structure difficult to observe. Certainly there is appreciable bound-bound absorption in this region as well as bound-free absorption. The bound-bound excitation leads predominantly to molecular fluorescence which is not efficiently detected through the narrow-band atomic line filters. The profile peaks near $\sim$560 nm in agreement with predictions based on calculated bound-free Franck-Condon factors[25] using hybrid [RKR (Rydberg-Klein-Rees), *ab initio*, R^{-6}] potential-energy curves.[20–23] This comparison between the theoretically predicted thermally averaged bound-free absorption spectrum (solid line) and the experimentally observed (D_1+D_2) excitation spectrum (circles) is given in Fig. 2. This spectral region is relatively free from competing absorption[15,19] in Na_2 and K_2. In particular, the $K_2(X\,^1\Sigma_g^+ - B\,^1\Pi_u)$ photodissociation profile extends over the range from $\sim$600–640 nm. The far-red spectral region observed here, beyond 580 nm, may have some slight overlap with the K_2 absorption spectrum. Figure 3 shows the D_1/D_2 branching ratio as a function of laser wavelength. This fine-structure branching ratio is a strong function of wavelength varying from near zero to $D_1/D_2 \sim 25\%$ as the laser is tuned across the bound-free profile.

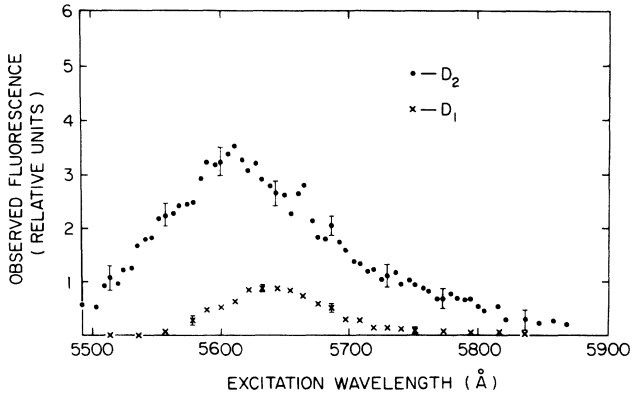

FIG. 1. Experimentally observed bound-free excitation spectrum leading to atomic fluorescence on the $K^*(4\,^2P_{3/2} - 4\,^2S_{1/2}(D_2))$ line or the $K^*(4\,^2P_{1/2} - 4\,^2S_{1/2}(D_1))$ line.

This branching ratio is unexpectedly large. Experimental tests to verify that the observed branching is not contaminated by experimental artifacts have been carried out. The D_1/D_2 ratio is independent of laser power. We have verified that the observed D_1 signal is not due to D_2 emission leakage through the D_1 filter by scanning the emission spectrum with a monochromator. The D_1/D_2 branching ratio is independent of oven temperature and hence particle density in the beam over a range from $T_0 \sim 670$ to 770 K. Perhaps the most convincing test involves running the molecular beam with pure K_2 and shifting the laser wavelength into the $K_2(X\,^1\Sigma_g^+ - B\,^1\Pi_u)$ photodissociation region beyond 600 nm. Under otherwise identical experimental conditions, we detect no observable $K^*(4\,^2P_{1/2}(D_1))$ emission in agreement with earlier studies of K_2 photodissociation.[15,19] Thus there is no observable effect of fine-structure changing collisions following the dissociation.

It is difficult to entirely rule out collision-induced dissociation of bound excited states;[13] the process is thought

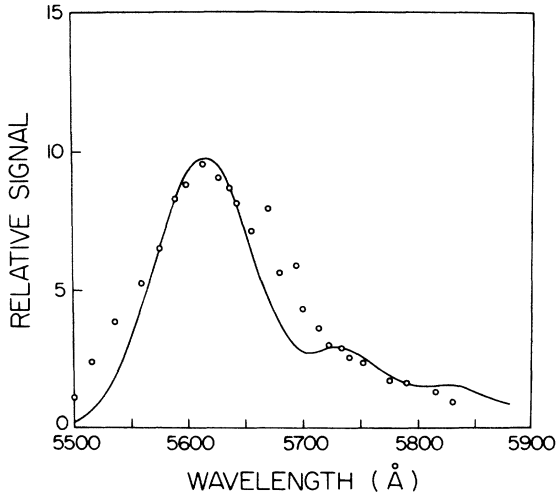

FIG. 2. Comparison of the theoretically predicted thermally averaged NaK($X\,^1\Sigma^+ - B\,^1\Pi$) absorption spectrum (solid curve) with the experimental spectrum (D_1+D_2 emission).

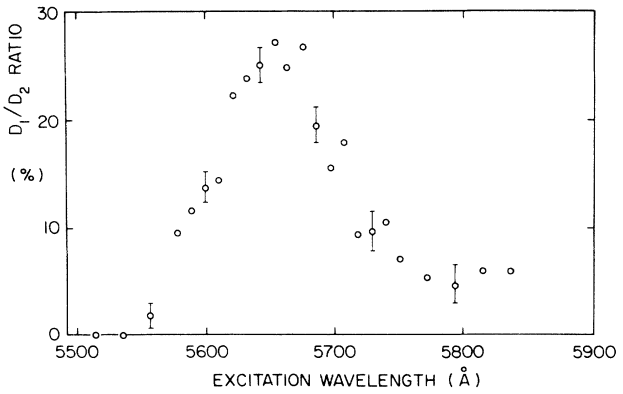

FIG. 3. Experimentally observed D_1/D_2 branching ratio vs excitation wavelength.

to have a large cross section[26] but has not been well studied. While beam-background gas interactions are certainly negligible, collisions within the beam are a possible source of concern. However, as discussed, the D_1/D_2 branching ratio is independent of beam density. Furthermore, fine-structure mixing collisions and collision-induced dissociation of K_2 have been demonstrated to be negligible. It seems unlikely that collision-induced dissociation cross sections for NaK would be significantly larger than for these processes.

III. DISCUSSION

The long-range adiabatic correlations for the excited states of NaK are given in Table I. These predictions differ from those given by Kato and Noda[14] for the adiabatic correlations based on the state ordering at short range ($R < 9a_0$). In this case the free-state wave packet will traverse the short-range crossings (Fig. 4) diabatically to the long-range limit beyond $\sim 13a_0$. In this region the adiabatic correlations of Table I are appropriate. The photodissociation process is clearly not completely adiabatic. We have carried out a semiclassical (classical trajectory) model calculation of the dissociation, numerically integrating the Schrödinger equation in the molecular frame following excitation of the $B\ ^1\Pi$ molecular state. The method is similar to that described by Gordeev, Nikitin, and Shushin,[18] but our calculation includes both spin-orbit and rotational-coupling terms[27] and uses the *ab initio* potential-energy curves of Stevens, Konowalow, and Ratcliff.[22] The Hamiltonian matrix (7×7) in the rotating molecular frame can be written

$$H = H^{\rm es} + H^{\rm s.o.} + H^{\rm rot} .$$

The Hund's case (a) basis states are labeled 1–7 according to $^3\Pi(\Omega=2)$, $^3\Pi(\Omega=1)$, $^1\Pi(\Omega=1)$, $^3\Sigma^+(\Omega=1)$, $^3\Pi(\Omega=0)$, $^3\Sigma^+(\Omega=0)$, and $^1\Sigma^+(\Omega=0)$. The electrostatic Hamiltonian ($H^{\rm es}$) is diagonal with the diagonal elements given by spline fit functions to the *ab initio* data points of Ref. 22. The spin-orbit Hamiltonian elements are given by

$$H^{\rm s.o.}_{11} = -H^{\rm s.o.}_{55} = H^{\rm s.o.}_{23} = H^{\rm s.o.}_{24} = H^{\rm s.o.}_{56} = H^{\rm s.o.}_{57} = -H^{\rm s.o.}_{34} = \tfrac{1}{3}\varepsilon ,$$

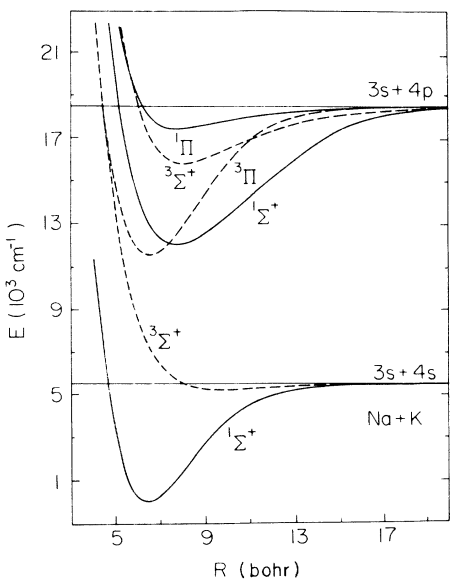

FIG. 4. NaK molecular potential-energy curves from Ref. 22.

where ε is the asymptotic spin-orbit splitting (57.7 cm^{-1}). The rotational-coupling elements are given by

$$H^{\rm rot}_{12} = H^{\rm rot}_{14} = H^{\rm rot}_{25} = H^{\rm rot}_{26} = H^{\rm rot}_{37} = H^{\rm rot}_{46} = \frac{+i}{\sqrt{2}}\dot{\theta} ,$$

where $\dot{\theta}$ is the time derivative of the classical deflection angle. The other elements are zero or given by the requirement that the Hamiltonian be Hermitian. A number of smaller effects (e.g., spin-spin, hyperfine coupling, etc.) have been neglected. The Schrödinger equation in the molecular frame

$$-i\hbar\frac{da_\nu(t)}{dt} = \sum_{\mu=1}^{7} H_{\nu\mu}(t)a_\mu(t) ,$$

coupled with the dynamical equations

$$\frac{dR}{dt} = v, \quad \frac{dv}{dt} = -\frac{1}{\mu}\frac{d\bar{V}(R)}{dR}$$

and

$$\dot{\theta} = \frac{J}{\mu\pi^2} ,$$

is then integrated using a Runge-Kutta routine to obtain the complex amplitudes $a_\nu(t)$ of the wave function in the molecular basis states. Here μ is the reduced mass and $\bar{V}(R)$ is the average potential defined as $\frac{1}{7}{\rm Tr}(H)$. The

TABLE I. Long-range adiabatic correlations. Assumes at long range the ordering of the states is given by $^1\Sigma_0^+ < {}^3\Sigma_{0,1}^+ < {}^3\Pi_{2,1,0} < {}^1\Pi_1$.

Molecular states	Atomic states
$A\ ^1\Sigma_0^+; b\ ^3\Sigma_{0,1}^+$	$\mathrm{Na}(3\,^2S_{1/2}) + \mathrm{K}^*(4\,^2P_{1/2})$
$b\ ^3\Pi_{2,1,0}; B\ ^1\Pi_1$	$\mathrm{Na}(3\,^2S_{1/2}) + \mathrm{K}^*(4\,^2P_{3/2})$

asymptotic wave function is then reexpressed in the atomic basis using Clebsch-Gordan algebra. Over the range of experimentally accessible energies ($E < 2000\ \mathrm{cm}^{-1}$) and rotational quantum numbers ($J \lesssim 180$), the predicted fine-structure branching to the D_1 level is always $\lesssim 10\%$. This value is significantly less than that observed experimentally near the peak of the bound-free profile ($\sim 25\%$).

We note that the spin-orbit coupling strength is a strong function of internuclear separation in this system. In the calculation we assumed the spin-orbit coupling parameter to be constant at its asymptotic value. However, in the small R regions the $^1\Pi - {}^3\Sigma^+$ spin-orbit coupling matrix elements have been measured and are estimated to be $\sim \frac{1}{2}$ of the asymptotic value.[28] Unfortunately the variation in the spin-orbit interaction as a function of internuclear separation has not been accurately determined.

Photodissociation via the $A\ ^1\Sigma^+$ state must be considered. Any wave packet excited at short range will pass the $^1\Sigma^+ - {}^3\Pi$ crossing diabatically, remaining on the $^1\Sigma^+$ curve which then correlates at long range with the D_1 level. To assess the possible role of direct excitation to the $A\ ^1\Sigma^+$ state, we have calculated the bound-free Franck-Condon factors for the $X\ ^1\Sigma^+ - A\ ^1\Sigma^+$ transition using hybrid (RKR, *ab initio*, R^{-6}) potential curves. The calculated Franck-Condon factors for photodissociation via the A state in this wavelength range are less than 10^{-4} of those calculated for the B state. Thus direct photodissociation via the A state is an unlikely explanation for the observed D_1 signal.

An additional complication arises since the $B\ ^1\Pi$ state and the $c\ ^3\Sigma^+$ state are predicted to have a crossing on the inner wall just above threshold (Fig. 4).[22] This may contribute to the anomalous D_1/D_2 branching ratio through direct excitation to the continuum of a "mixed" $^1\Pi - {}^3\Sigma^+$ state in the neighborhood of the crossing on the inner wall. The free-state wave packet will traverse the $^3\Sigma^+ - {}^3\Pi$ crossing primarily diabatically; we have estimated a Landau-Zener probability of $\sim 98\%$ for the diabatic passage. The $^3\Sigma^+$ state adiabatically correlates with the D_1 level at long range.

These dynamics can be further clarified by measurements of the atomic line polarization, through high-resolution studies of this excitation spectrum, and through initial-state selected experiments. Detailed modeling, however, will certainly require accurate knowledge of the variation of the spin-orbit coupling strength as a function of internuclear separation.

ACKNOWLEDGMENTS

This work has been supported by the National Science Foundation. We gratefully acknowledge helpful discussions with Dr. Paul Julienne and the loan of vacuum equipment from Dr. David Rethwisch.

*Also at the Center for Laser Science and Engineering and Department of Physics and Astronomy, The University of Iowa, Iowa City, Iowa 52242-1479.

[1]M. Shapiro and R. Bersohn, Ann. Rev. Phys. Chem. **33**, 409 (1982).
[2]S. R. Leone, Adv. Chem. Phys. **50**, 1225 (1982).
[3]C. H. Green and R. N. Zare, Ann. Rev. Phys. Chem. **33**, 119 (1982), and references therein.
[4]S. J. Singer, K. F. Freed, and Y. B. Band, J. Chem. Phys. **79**, 6060 (1983); S. J. Singer and K. F. Freed, in *Advances in Chemical Physics, LXI*, edited by I. Prigogine and S. A. Rice (Wiley, New York, 1985), and references therein.
[5]J. M. Brom and H. P. Broida, J. Chem. Phys. **61**, 982 (1974).
[6]D. L. Feldman and R. N. Zare, Chem. Phys. **15**, 415 (1976).
[7]V. B. Grushevskii, S. M. Papernov, and M. L. Yanson, Opt. Spektrosk. **44**, 809 (1978) [Opt. Spectrosc. **44**, 475 (1978)].
[8]G. Ennen and C. Ottinger, Chem. Phys. **41**, 415 (1979); **40**, 127 (1979).
[9]E. K. Kraulinya and M. L. Yanson, Opt. Spektrosk. **46**, 1112 (1979) [Opt. Spectrosc. **46**, 629 (1979)]; E. K. Kraulinya, S. M. Papernov, and M. L. Janson, Chem. Phys. Lett. **63**, 531 (1979).
[10]E. W. Rothe, U. Krause, and R. Düren, J. Chem. Phys. **72**, 5145 (1980).
[11]E. J. Breford and F. Engelke, Chem. Phys. Lett. **75**, 1132 (1980).
[12]C. Noda and H. Kato, Chem. Phys. Lett. **86**, 415 (1982).
[13]M. Allegrini, L. Moi, and E. Arimondo, Chem. Phys. Lett. **45**, 245 (1977).
[14]H. Kato and C. Noda, J. Chem. **73**, 4940 (1980).
[15]M. L. Janson and S. M. Papernov, J. Phys. B **15**, 4175 (1987).
[16]Z. Wu and J. Huennekens, J. Chem. Phys. **81**, 4433 (1984).
[17]J. G. Balz, R. A. Bernheim, W. J. Chen, and L. P. Gold, Chem. Phys. Lett. **115**, 353 (1985).
[18]E. A. Gordeev, E. E. Nikitin, and A. I. Shushin, Mol. Phys. **33**, 1611 (1977).
[19]V. Zafiropulos, P. D. Kleiber, K. M. Sando, X. Zeng, A. M. Lyyra, and W. C. Stwalley, Phys. Rev. Lett. **61**, 1485 (1988).
[20]A. J. Ross, C. Effantin, J. D'Incan, and R. F. Barrow, Mol. Phys. **56**, 903 (1985); A. J. Ross, R. M. Clements, and R. F. Barrow, J. Mol. Spec. **127**, 546 (1988); R. F. Barrow, R. M. Clements, J. Derouard, N. Sadeghi, C. Effantin, J. D'Incan, and A. J. Ross, Can. J. Phys. **65**, 1154 (1987); R. F. Barrow, R. M. Clements, G. Delacretaz, C. Effantin, J. D'Incan, A. J. Ross, J. Verges, and L. Wöste, J. Phys. B **20**, 3047 (1987); A. J. Ross, C. Effantin, J. D'Incan, and R. F. Barrow, *ibid.* **19**, 1449 (1986).
[21]G. H. Jeung, J. P. Daudey, and J. P. Malrieu, Chem. Phys. Lett. **94**, 300 (1983).
[22]W. J. Stevens, D. D. Konowalow, and L. B. Ratcliff, J. Chem. Phys. **80**, 1215 (1984); L. B. Ratcliff and D. D. Konowalow, J. Mol. Spec. **110**, 242 (1985).
[23]B. Bussery and M. Albert-Frecon, J. Phys. B **18**, L379 (1985).
[24]P. W. Arcuni, M. L. Troyer, and A. Gallagher, Phys. Rev. A

41, 2398 (1990).
[25]P. S. Herman and K. M. Sando, J. Chem. Phys. **68**, 1153 (1978);
[26]K. Bergmann, W. Demtröder, M. Stock, and G. Vogl, J. Phys. B **7**, 2036 (1974).
[27]See also, for example, L. J. Kovalenko, S. R. Leone, and J. B. Delos, J. Chem. Phys. **91**, 6948 (1989), and references therein.
[28]P. Kowalczyk, J. Chem. Phys. **91**, 2779 (1989).